JOURNAL OF GEOPHYSICAL RESEARCH, VOL. 106, NO. E12, PAGES 32,777–32,795, DECEMBER 25, 2001

The roughness of natural terrain: A planetary and remote sensing perspective

Michael K. Shepard,[1] Bruce A. Campbell,[2] Mark H. Bulmer,[2] Tom G. Farr, [3] Lisa R. Gaddis, [4] and Jeffrey J. Plaut[3]

Abstract. We examine the various methods and parameters in common use for quantifying and reporting surface topographic "roughness." It is shown that scale-dependent roughness parameters are almost always required, though not widely used. We suggest a method of standardizing the parameters that are computed and reported so that topographic data gathered by different workers using different field techniques can be directly and easily intercompared. We illustrate the proposed method by analyzing topographic data from 60 different surfaces gathered by five different groups and examine the information for common features. We briefly discuss the implications of our analysis for studies of planetary surface roughness, lander safety, and radar remote sensing modeling and analysis.

1. Introduction

Surface roughness, as discussed in this paper, is defined as the topographic expression of surfaces at horizontal scales of millimeters to a few hundred meters. These are the scales with which the field geologist is most familiar and are therefore of value to those studying the geology of the Earth or terrestrial planets. These same scales also have the greatest effect on the behavior of scattered microwaves (radar) and are therefore of interest to any geologist interpreting radar remote-sensing data. In the past few decades the quantitative characterization of surface roughness has become increasingly important. Geologists may wish to compare the roughness of one terrestrial lava flow to another [e.g., *Gaddis et al.*, 1990]. Planetary geologists may wish to compare the roughness of one Venusian plains unit to another or to a terrestrial analog [e.g., *Campbell and Campbell*, 1992; *Plaut and Arvidson*, 1992]. In remote sensing, it is often necessary to utilize one or more roughness parameters extracted from a scattering model applied to observations of the planetary surface. Geomorphologists may seek to understand how landforms evolve by numerically simulating a natural landscape, subjecting that landscape to various processes, and studying the result [e.g., *Chase*, 1992, *Farr*, 1992; *Luo et al.*, 1997; *Howard and Craddock*, 1998]. Forward modeling of this type can provide insights into the role of erosion, deposition, and climatic variation (among others) in the modification of these surfaces. In all of these endeavors, some method of quantitatively characterizing surfaces must be utilized.

[1]Department of Geography and Geosciences, Bloomsburg University, Bloomsburg, Pennsylvania, USA.
[2]Center for Earth and Planetary Studies, National Air and Space Museum, Washington, D.C., USA.
[3]Jet Propulsion Laboratory, Pasadena, California, USA.
[4]U. S. Geological Survey, Flagstaff, Arizona, USA.

Paper number 2000JE001429.
0148-0227/01/2000JE001429$09.00

There are two historical approaches to quantify surface roughness. The first and simplest is to assume a mathematically tractable form, often of a statistical nature. For example, in the development of radar and optical scattering models it is common to assume a stationary surface (one for which statistical parameters such as the mean and standard deviation do not change over any measured scale) characterized by a zero mean, constant standard deviation, and constant autocorrelation length. Unfortunately, it turns out that this is a rather poor model for most naturally occurring surfaces. The second approach is to physically measure and catalog the topographic expression of various surfaces without a priori assumptions about its form. While this approach should produce a realistic quantitative characterization of natural terrain, many workers continue to implicitly assume that the surface is stationary and to utilize a single measure of the standard deviation or other roughness parameter.

There is currently no standard method for quantitatively characterizing surface roughness. In large part this is because different investigators use a variety of measurement techniques. Common techniques include the use of laser profilers [*Campbell and Garvin*, 1993], line and transit [*Campbell and Garvin*, 1993; *Anderson et al.*, 1998], mechanical profilers [*Gaddis et al.*, 1990], stereophotography [*Farr*, 1992; *Arvidson et al.*, 1991; *Helfenstein and Shepard*, 1999], and differential GPS [*Bulmer and Campbell*, 1999]. Profile lengths in these investigations range from a few centimeters to hundreds of meters; measurement intervals range from a submillimeter to tens of centimeters or more. Methods of reporting or characterizing the surface differ just as widely. Some report the slope and offset of power spectra, others report the root-mean-square (RMS) height of a detrended profile, while still others report the autocorrelation length, RMS slope, or some combination of the above parameters.

Measurement techniques will continue to differ depending upon the scales of interest, resources available to the investigators, and advances in technology. What is presently lacking, but is attainable, is a simple, intuitive, and

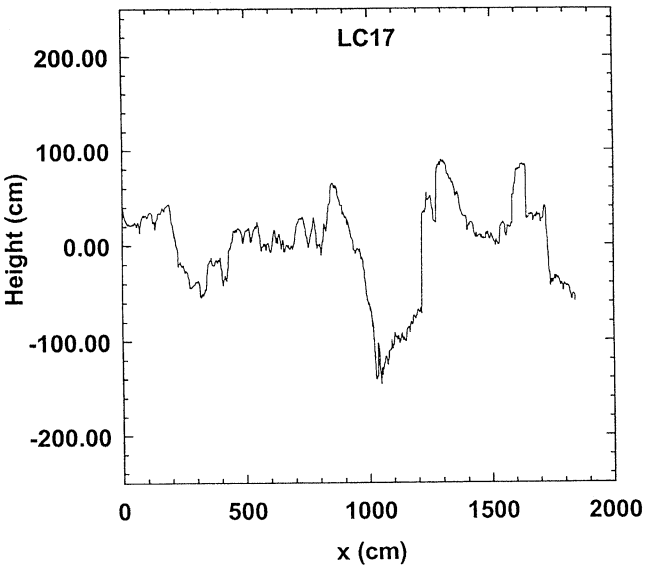

Figure 1. Profile of the rough a'a flow LC17 in the Lunar Crater Volcanic Field, Nevada. Vertical exaggeration is a factor of 4.

standardized method for analyzing and reporting the results of roughness measurements so that direct intercomparisons can be made between data sets. The purpose of this paper is twofold: (1) to propose such a method and to demonstrate its application to a variety of different measurement techniques and surfaces and (2) to compile a significant reference data set of terrestrial surface roughness and to explore it for unifying features. We first discuss commonly reported roughness parameters and propose a simple method of standardization. While we concentrate in this paper specifically on scales of a centimeter up to a few tens of meters, the methods we propose are of use for any range of scales. Next, this method will be illustrated using data acquired by a variety of techniques at numerous field sites and summarized in a format suitable for use as a reference. Finally, we will compare the surfaces in this data set, look for commonalties, and examine a few of the implications for remote sensing and planetary investigations.

2. Mathematical Characteristics of Natural Topography

A number of different parameters have been used to quantitatively model surface roughness. Here we will illustrate those most commonly used by the planetary and radar remote-sensing communities using the profile of an a'a basalt flow (LC17) in the Lunar Crater Volcanic Field, Nevada. This profile is one of 15 acquired at this site using helicopter stereophotography during the Geologic Remote Sensing Field Experiment (GRSFE) [*Farr*, 1992; *Arvidson et al.*, 1991] and is ~18 m long. Surface height samples were taken every (horizontal) centimeter, and the vertical accuracy is estimated to be a few millimeters (Figure 1).

2.1. Commonly Reported Roughness Parameters

2.1.1. Root-mean-square height. The most commonly reported parameter, and the simplest to obtain, is the root-mean-square (RMS) height, or the standard deviation of heights about the mean. Often the profile is first "detrended" by subtracting a best fit linear function from the data, leaving a series of heights with a mean value of zero. We will discuss the validity of this process later. The RMS height, ξ, is given by

$$\xi = \left[\frac{1}{n-1}\sum_{i=1}^{n}\left(z(x_i)-\bar{z}\right)^2\right]^{1/2}, \quad (1)$$

where n is the number of sample points, $z(x_i)$ is the height of the surface at point x_i, and $\bar{z}$ is the mean height of the profile over all x_i. For the profile in question the RMS height is 47.8 cm over its full 18-m length.

2.1.2. Root-mean-square deviation. The RMS or Allan deviation, v, is related to the Allan variance, variogram, or structure function. It is defined as the RMS difference in height between points separated by a lag or step, Δx, and given by

$$v(\Delta x)=\left\{\frac{1}{n}\sum_{i=1}^{n}\left[z(x_i)-z(x_i+\Delta x)\right]^2\right\}^{1/2}. \quad (2)$$

As we will discuss in more detail in section 2.2.2, it is a function of the lag or step size, Δx. At the 1 cm scale for the flow in Figure 1, $v = 3.7$ cm.

2.1.3. Root-mean-square slope. Another commonly reported parameter is the RMS slope, s_{rms}, which is the RMS deviation divided by the step size, Δx,

$$s_{\mathrm{rms}}=\frac{v(\Delta x)}{\Delta x}. \quad (3)$$

It is common for the RMS slope to be reported in degrees, θ_{rms}, where $\theta_{\mathrm{rms}} = \tan^{-1}(s_{\mathrm{rms}})$. As with the RMS deviation, the RMS slope is a function of the scale, Δx, at which it is measured. Often, however, one will find the RMS slope reported only for a single scale, usually the smallest sample interval obtained on the profile (although this is not always stated explicitly). For this profile the slope at 1 cm spacing is $\theta_{\mathrm{rms}} = 74.9°$. Slope distributions calculated along a profile line are termed unidirectional. In contrast, the adirectional RMS slope represents the distribution of maximum tilt (i.e., the gradient of the topographic contours) at each point on a three-dimensional surface. For a Gaussian-distributed set of surface slopes the adirectional value is $\sqrt{2}$ greater than the unidirectional value.

2.1.4. Autocorrelation length. The autocorrelation function of a profile is the normalized covariance between the profile and itself when offset by some step or lag, Δx [cf. *Turcotte*, 1997]. The autocorrelation is, by definition, equal to 1.0 when the lag is zero. The autocorrelation length (also referred to simply as the correlation length), l, is usually defined as the distance or lag required to reduce the normalized correlation value to $1/e$, or ~37%. Smoother surfaces generally have large autocorrelation lengths, while rough surfaces have low values of l. A profile of white noise has an autocorrelation length of zero, while a straight horizontal line has an autocorrelation length of infinity. The autocorrelation length for the sample profile, using its full 18-m length, is 1.32 m.

2.1.5. Effective slope. It is not uncommon, especially in radar-scattering models, for the roughness of the surface to be defined as the ratio of the RMS height to the autocorrelation length (or some variant of this ratio) [e.g., *Miller and Parsons*, 1990]. In many instances, this ratio is confusingly referred to as the RMS slope; however, it is not the same measure as the RMS slope given by (3). To mitigate the confusion, *Campbell and Garvin* [1993] suggested the use of the term "effective slope," s_{eff}, given by

$$s_{\text{eff}} = \frac{\xi}{l}. \tag{4}$$

As with the RMS slope, the effective slope is often reported in degrees where $\theta_{\text{eff}} = \tan^{-1}(s_{\text{eff}})$. The effective slope for the sample profile is $\theta_{\text{eff}} = 19.9°$.

2.1.6. Median and absolute slope. Some have suggested that the RMS slope is a poor representation of a profile's true behavior because outlying points or a long-tailed slope frequency distribution will bias the RMS slope toward higher values [cf. *Kreslavsky and Head*, 1999]. To mitigate the effects of a few high or erroneous slopes, one can use either the absolute slope, given by

$$s_{\text{abs}} = \frac{1}{\Delta x}\left\{\frac{1}{n}\sum_{i=1}^{n}\left|z(x_i) - z(x_i + \Delta x)\right|\right\}, \tag{5}$$

or the median slope, s_{med}, which is simply the median (value above and below 50% of the total population) of the absolute slopes of the surface (without taking the absolute value of slopes, the median slope of a detrended profile would be near zero). As with other slope measures, these are commonly reported in degrees, $\theta_{\text{abs}}=\tan^{-1}(s_{\text{abs}})$ and $\theta_{\text{med}}=\tan^{-1}(s_{\text{med}})$.

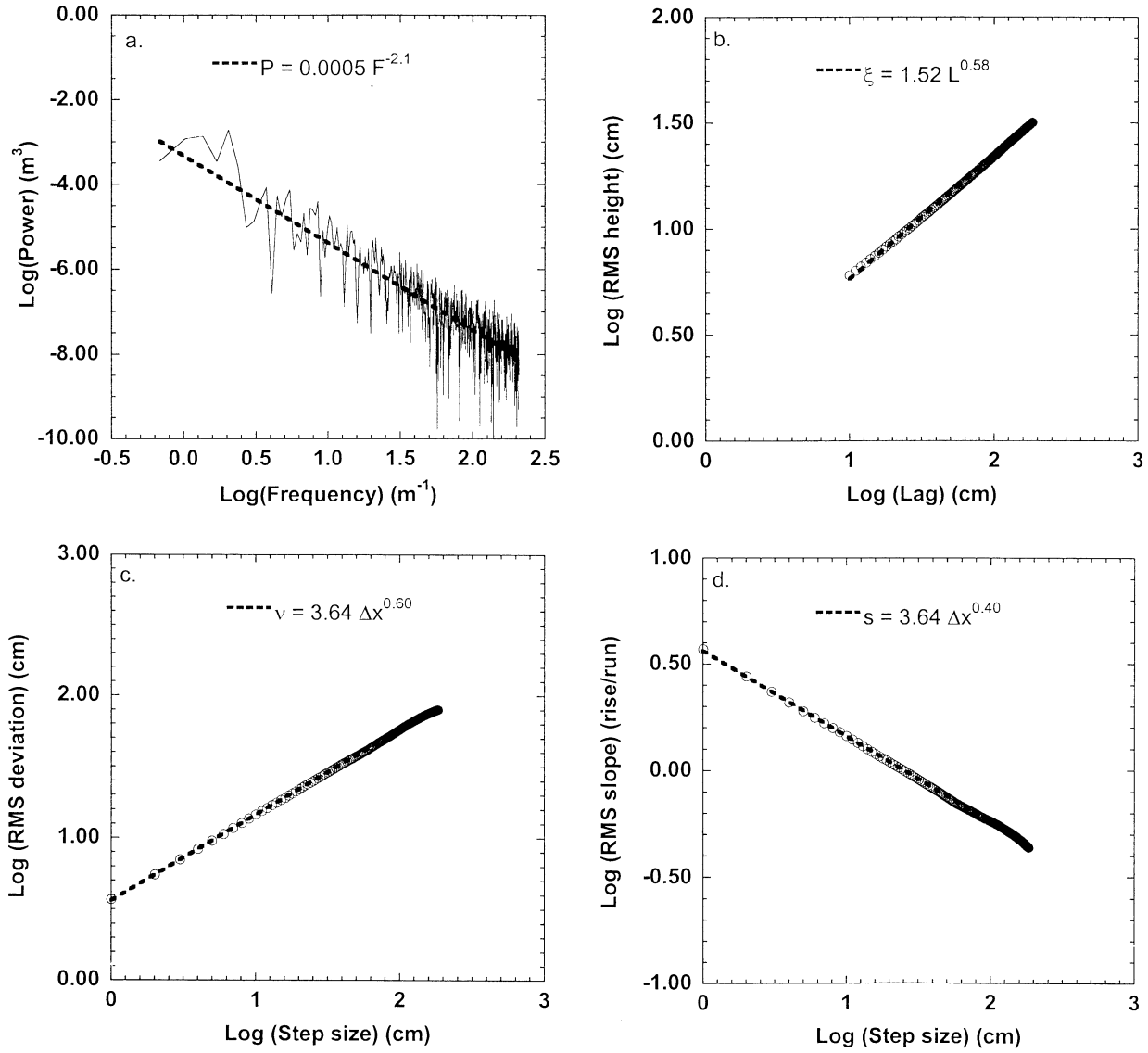

Figure 2. Different methods of characterizing the scale-dependent roughness of a surface using LC17 (Figure 1) as an example. Equations represent best fit lines through the data. (a) Power spectrum. (b) Average RMS height versus profile length. (c) RMS deviation versus lag or step interval. (d) RMS slope versus lag or step interval. Note that the spatial methods (Figures 2b, 2c, and 2d) are much "cleaner" than the power spectral method (Figure 2a).

For the sample data at 1 cm scale, θ_{abs} = 54.6° and θ_{med} = 37.4°.

2.1.7. Power spectrum. The power spectrum of a profile is a measure of the "power" present in each discrete spatial frequency sampled by the data and is given by the magnitude of the Fourier transform (FT) of the profile. The power spectrum is often approximately linear when plotted on a logarithmic scale and can be fit with a power law (straight line on log-log scale). The slope and intercept of this line are occasionally reported as roughness parameters [e.g., *van Zyl et al.*, 1991]. Figure 2a shows the power spectrum of the sample data. Unfortunately, there is no simple correspondence between the intercept or slope of the best fit line to the power spectrum and any of the previously reported roughness measures.

2.2. Necessity of Considering Scale

With the exception of the power spectrum, all of the methods discussed above are deficient for characterizing surface roughness because they do not take into account the scale dependence inherent in natural surfaces. As noted in section 1, most models of surface roughness or topography assume that the surface is stationary. Mathematically, this implies that statistical parameters such as the mean and standard deviation are constant and independent of the scales over which they are measured. White noise is an example of a stationary surface. However, it is now well established that the roughness of natural surfaces is nonstationary [*Sayles and Thomas*, 1978; *Mandelbrot*, 1982; *Turcotte*, 1997; *Shepard et al.*, 1995]. At a minimum, quantitative characterizations of natural surfaces will require two parameters, like the slope and offset of the power spectrum. Unfortunately, the power spectrum presents roughness information in frequency space and is neither intuitive nor easily related to any other parameter discussed. However, at least three spatial analogs to the power spectrum exist, which we illustrate in sections 2.2.1-2.2.3.

2.2.1. RMS height versus profile length. If we measure the RMS height of our sample lava flow at different scales, we find that it increases with profile length. A logarithmic plot of this behavior is shown in Figure 2b. The RMS height plotted at any given scale is the square root of multiple averaged height variances; that is, one can obtain at least 100 estimates of the height variance at the 10-cm scale from a 1000-cm-long profile. Also shown in Figure 2b is a best fit power law to the data (straight line on this graph), given by

$$\xi(L) = \xi_0 L^H, \tag{6}$$

where L is the length of the profile, H is a scaling parameter called the Hurst exponent (or sometimes Hausdorff dimension) ($0 \le H \le 1$), and ξ_0 is the RMS height of the profile at unit scale, in this case at a scale of 1 cm. This type of scaling behavior is observed from virtually all natural topography and is loosely referred to as "fractal" [cf. *Mandelbrot*, 1982; *Turcotte*, 1997, *Shepard et al.*, 1995]. More precisely, the behavior exhibited is "self-affine," which indicates that the roughness in the vertical direction increases at a fixed, slower rate than the horizontal scale at which it is measured. The special case H=1 is called "self-similar" because the horizontal and vertical dimensions scale at the same rate. The Hurst exponent is related to the fractal dimension, D, by

$$\begin{aligned} &\text{Profile} && D = 2 - H \\ &\text{Surface} && D = 3 - H, \end{aligned} \tag{7}$$

where the top relationship refers to the fractal dimension of a profile and the bottom refers to the fractal dimension of a surface. We will generally use the Hurst exponent and avoid using the fractal dimension.

2.2.2. RMS deviation versus step interval. The RMS deviation of natural terrain, like the RMS height, often follows a power law trend with horizontal scale, but that scale is set by the distance between successive points:

$$\nu(\Delta x) = \nu_0 (\Delta x)^H, \tag{8}$$

where Δx is the step size and ν_0 is the RMS deviation at the unit scale. The scaling parameter H is the same as that in (6). Figure 2c shows a best fit plot of (8) with the sample data.

2.2.3. RMS slope versus step interval. The RMS slope is a close relative of the RMS deviation, as illustrated by (3). Not surprisingly, the RMS slope, s_{rms}, also varies with step size as

$$s_{rms}(\Delta x) = s_{rms,0} (\Delta x)^{1-H}. \tag{9}$$

Figure 2d shows the best fit power law with the sample data and reveals the same value for H as found in Figures 2b and 2c. The intercept, $s_{rms,0}$, is the value of the RMS slope at a step of one unit, in this case, 1 cm.

2.2.4. Others. Numerous other parameters, such as the absolute or median slope, could be plotted in similar fashion and would give similar results. This is not often done, however, because these parameters are awkward to include in a mathematical model of surface roughness. In addition, the autocorrelation function is known to depend on the profile length over which it is measured, so there is no single value for l [cf. *Shepard et al.*, 1995]. The effective slope appears to be the one spatial parameter which occasionally exhibits independence of scale but only when the RMS height and autocorrelation length vary with scale in a similar fashion [cf. *Shepard et al.*, 1995; *Campbell and Garvin*, 1993]. However, because the effective slope is a ratio of two parameters, surfaces with very different roughness behavior can take on the same value; for that reason, we will not pursue this parameter further.

2.3. More Complex Behavior

In section 2.2. we discuss how the RMS height, deviation, and slope are observed to vary with the scale at which they are measured. The model ideal is a strict power law which holds over all scales. However, it is obvious that this behavior must break down at some scales: surfaces do not continue to roughen infinitely at smaller scales, nor do they increase to indefinitely large scales. Figure 2 illustrated the ideal behavior

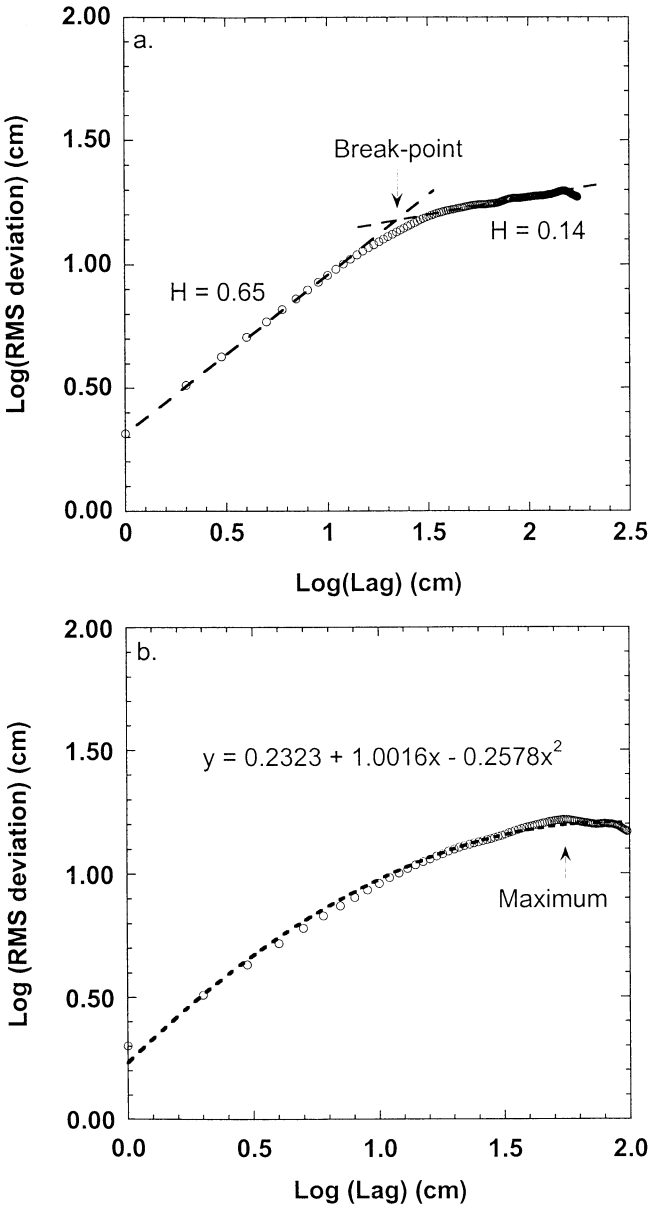

Figure 3. Deviograms (RMS deviation version lag) of more "typical" profiles. (a) A surface (DV12) which exhibits one Hurst exponent from the smallest scale up to a breakpoint at which point the Hurst exponent rapidly changes to a different value. (b) A more complex deviogram (also from DV12) better described with a polynomial and a maximum RMS deviation believed to be related to periodic behavior of this scale length on the surface.

over a limited range of scales. Figure 3a shows a plot of RMS deviation versus scale (referred to hereinafter as a deviogram) for a more typical profile (from DV12, an extremely rough, eroded surface). Here it will be seen that the power law behavior holds from the smallest scale up to a horizontal scale of 23 cm, at which point it appears to "break over" and obey a different power law. The scale at which the break over occurs is thought to be related to a transition in the processes that form or modify the surface being investigated. For example, *Campbell and Shepard* [1996] noted that on a Hawaiian pahoehoe flow, the roughness at centimeter scales was dominated by the weathering and erosion of a glassy rind, while at meter scales the roughness was dominated by flow emplacement mechanisms, e.g., ropy structures and other flow features. In many cases, the break over point is relatively clear (for this example, ~23 cm); in others, there is a slow transition, and the entire plot would more precisely fit by a polynomial than a series of lines (Figure 3b, also a profile from DV12). Detrending the data (discussed in section 3.1.1) may also introduce some level of break over. However, this effect should be minimized by limiting the scales of investigation to ≤10% of the overall profile length.

3. Proposed Method of Standardizing Roughness Information

3.1. Data Preparation

The most common form of roughness data is the profile, a set of heights measured at equally spaced intervals along a straight line. More uncommon, but of greater value, are gridded arrays of points at equally spaced intervals. Both types of data are analyzed in similar fashion, but gridded data allow one to measure roughness along different azimuths and determine to what extent the surface is isotropic. Visual inspection, either in the field or from photographs, can also provide a qualitative estimate of anisotropy.

3.1.1. Detrending the data and filtering. To detrend data, a best fit line (or plane for a grid) is subtracted from the data so that the profile has a mean of zero. The major reason for doing this is to emphasize the overall variation of the "small-scale" terrain from a general trend. Here we use the term small-scale to mean horizontal scales smaller than ~10% of the overall profile length, while "large-scale" refers to those between 10% and 100% of the profile length. In some cases, as with profiles obtained from helicopter-derived stereophotography, the profiles are tilted because the helicopter platform was tilted in flight. The amount of tilt is generally unknown but can be removed by detrending if one assumes the overall trend of the terrain is "level."

It can be argued, with some validity, that detrending removes important information about the surface. Removing the overall trend means that the large-scale roughness of a surface will be systematically smaller than in the raw profile. The greater the slope removed during detrending, the greater the discrepancy. However, the small-scale roughness is affected very little by detrending, unless the slope removed is particularly severe. Figure 4 illustrates this by showing the deviograms of a raw and detrended profile of a Hawaiian lava flow. Figure 4a compares the deviograms when the total slope removed is just under 2°. Note that at small scales the two plots are virtually indistinguishable and only begin to diverge at larger scales. Figure 4b shows deviograms for raw and detrended profiles of a surface with nearly twice the slope of Figure 4a. In this case, the divergence is more significant, even at smaller scales. Which profile is the more "correct"? The slope being removed is an artificial bias in the profile that results from undersampling the true surface. A downward slope in nature will always be found with an associated upward slope, even if on the other side of a mountain. Without compensating upward slopes to mitigate the effect of the downward trend in the deviogram, all roughness measures will

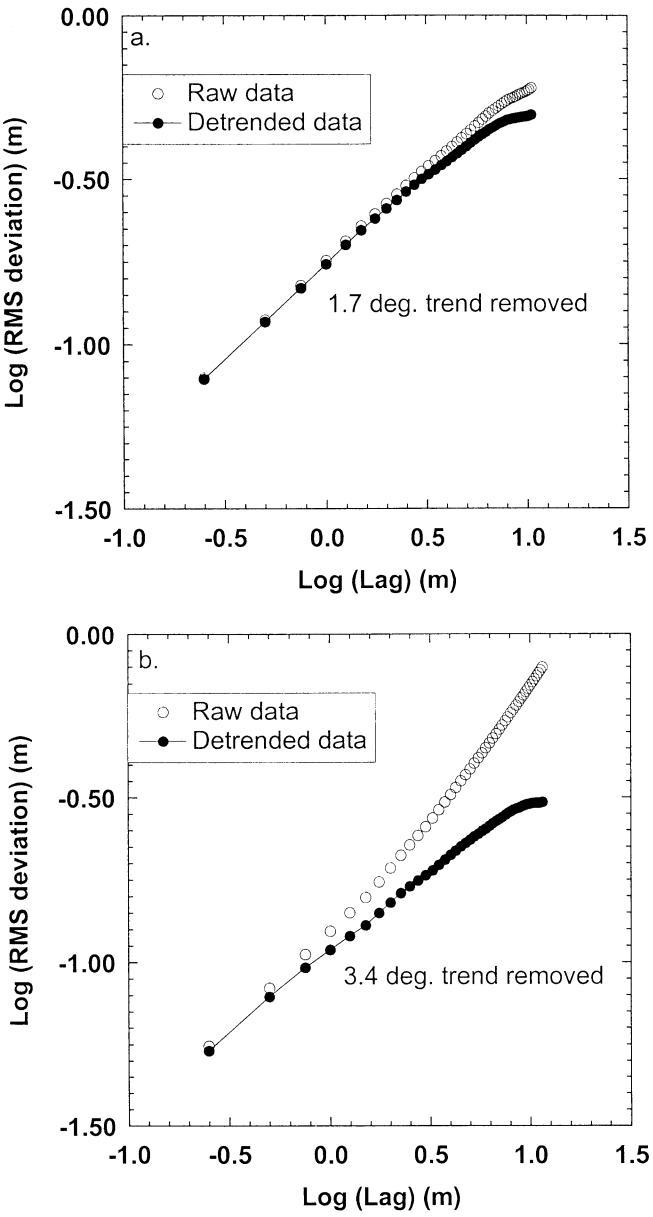

Figure 4. Deviograms of "raw" and detrended topographic data. (a) A slope of 1.7° removed from the raw profile to give the detrended profile. Note that the deviograms remain similar at small scales and begin to diverge at larger scales. (b) A slope of 3.4° removed to give the detrended profile. Here the divergence between deviograms begins at smaller scales than in Figure 4a because of the larger trend removed.

be biased high, and there is no reason to believe that the downward (or upward) trend in any topographic data is representative of all profiles of that length on similar terrain; it is only a sample of one. The process of detrending is therefore a convenient, but approximate way to remove some of the bias.

Filtering is common when calculating power spectra because low-frequency (long-wavelength) information tends to leak into the higher-frequency part of the unfiltered spectrum [*Austin et al.*, 1994]. Spatial methods suffer from a related difficulty due to the bias introduced by an overall slope in the data. Detrending is therefore a type of filtering operation and is the only type we can recommend.

3.1.2. Interleaving. Interleaving is the preferred method for generating plots of a given statistic versus scale. It refers to the way in which two points on a surface are chosen and compared. Consider, for example, a 10-m profile with a 1-cm sample interval. To calculate the RMS slope of this profile at a step or lag of 10 cm, we start with points at 0 cm and 10 cm, then 10 cm and 20 cm, and so on until we reach 990 cm and 1000 cm. If we stop here, we have utilized only one-tenth of the information available. We could also calculate slopes from points at 1 cm and 11 cm, 11 cm and 21 cm, etc., and then begin again at 2 cm and 12 cm, 12 cm and 24 cm, and so on until our first point became 10 cm. The RMS slope at a scale of 10 cm is then computed based on all of these points.

The downside of interleaving is the illusion, especially at large scales, that our estimate of roughness is based on a large number of random samples. This is not true because, in general, adjacent points on a profile are correlated. For example, with the same 10-m profile discussed above, we can calculate an RMS slope for the surface at a scale of 5 m using a total of 499 estimates (0 cm and 500 cm, 1 cm and 501 cm, etc.). However, there will be little difference between slopes estimated by pairs of points separated by even a few tens of centimeters. If we want a realistic estimate of the RMS slope at scales of 5 m, then we need a much longer profile. As a general rule, the profile length should be a minimum of 10 times the length of the largest scale we wish to investigate.

The RMS height can also be interleaved, in a sense, by using a running boxcar filter over the data. For example, the RMS height at 10 cm may be calculated by taking the root of the average variance of samples consisting of all points between 0 cm and 10 cm, 1 cm and 11 cm, 2 cm and 12 cm, etc.

3.2. Parameters to Compute and Report

The following is a list of parameters and scales that we suggest should be reported wherever possible. In addition to these parameters, the profile length and sample interval should always be reported. The profile length will give one a sense of the maximum scale from which statistics can be safely extracted. The sample interval provides the minimum scale for which RMS deviation and slope can be obtained. If the profile is detrended before statistics are computed, then this should be reported along with the overall slope of the removed trend. If height data are available in orthogonal directions, as on a grid or perpendicular profiles, these parameters should be computed in both directions and compared. Significant differences can arise if the topography is anisotropic, as with surfaces generated or modified by directional processes (some lava flows, fluvial erosion, etc.).

3.2.1. RMS height. If desired, one may make a plot like Figure 2b. However, at a minimum, we suggest calculating the RMS height at "powers of 10," (e.g., 0.1 cm, 1 cm, 10 cm) up and down to the limits of the data. Although one can calculate an RMS height with as few as three data points, it seems prudent to utilize more wherever possible. For example, some of the data we examine below were taken at 25 cm intervals along ~100-m transects. We can estimate the RMS height for

these profiles at a scale of 1 m, but we can only utilize five points in any single estimate.

3.2.2. RMS deviation or slope. Either of these parameters is sufficient, since one can be easily computed from the other. Our preference is to make a deviogram like Figure 2c to compute the Hurst exponent (see section 3.2.3). However, the RMS slope is the more commonly used parameter. Like the RMS height, we suggest calculating and reporting the RMS slope at powers of 10. Unlike the RMS height, the RMS slope can be computed at the sample interval (i.e., between two adjacent points) and is therefore more convenient for investigating the smallest scales of roughness.

3.2.3. Hurst exponent and breakpoint scales. The deviogram is the simplest tool for computing the Hurst exponent. For two reasons, it is recommended that scales of less than one-tenth of the profile length be used to generate the deviogram. First, if the height data have been detrended, then the estimated RMS deviation may diverge significantly from the raw value at larger scales, thus skewing the estimated exponent. Second, the statistics at larger scales are poor due to the very limited sample size. The Hurst exponent should be estimated based on the deviogram behavior from the smallest scales up. If there is an obvious change in the Hurst exponent at larger scales, the new value should be estimated and the scale at which this change occurs, or breakpoint, should be noted. In some cases, the deviogram may be quite complex and not conform to this simple model behavior. In these cases, it is left to the investigator how best to proceed.

3.2.4. Uncertainties. Wherever possible, estimated uncertainties in the individual heights should be reported. These should also be propagated through the analysis to result in estimated uncertainties in RMS height and slope. More difficult to estimate are uncertainties in Hurst exponent. If a single Hurst exponent is evident in the deviogram, then the goodness of fit is easily estimated by least squares techniques. If a breakpoint is evident, however, the investigator must somewhat subjectively choose where the beginning and endpoints of each trend lie. This, in turn, will have an effect on estimated location of the breakpoint, found from the intersection of the two best fit lines. In the data described in section 4, we allow for this subjectivity with conservative (i.e., large) uncertainties reported for both Hurst exponents (±0.05) and the scale of breakpoints (±20%).

4. Application to Diverse Data Sets

4.1. Introduction to the Data Sets

The data sets described here were gathered by the coauthors, and most have been published in some form. The purpose of this section is to demonstrate the proposed method of standardizing roughness parameters and illustrate how it leads to consistent results that allow intercomparisons. Here we briefly describe the methods by which each data set was acquired and their applicable scales. Table 1 lists the file names of each profile examined, a brief description of the unit from which it was acquired, and the roughness parameters suggested in the section 3. In addition, notes accompanying Table 1 include the method of acquisition, sample interval, profile length, uncertainties in each parameter, and extend of detrending.

4.1.1. Helicopter-borne stereophotography. *Wall et al.*, [1991], *Farr* [1992] and *Arvidson et al.*, [1991] discuss in great detail the collection of this data set. Essentially, two fore and aft boom-mounted 70-mm cameras were flown by helicopter over sites of interest during several geologic field experiments (baseline of ~7 m). The stereopairs were reduced into a series of profiles at each site. Typically, 10 profiles of 10 m each and five profiles of 20 m each (orthogonal to the first 10), were produced from each stereopair. The horizontal resolution is 1 cm, and vertical uncertainties are estimated to be a few millimeters [*Farr*, 1992]. In a few instances, gridded arrays of points separated by 5 cm were produced. Because the helicopter was usually tilted during flight, there is an unknown tilt to each stereopair that is removed by detrending all profiles. Stereopairs were acquired over a wide variety of geologically interesting sites in Death Valley, California, and Lunar Crater Volcanic Field, Nevada, ranging from a'a flows, to alluvial fans, to playas. Twenty-five sites, each with 15 profiles, are examined in this paper.

4.1.2. Mechanical profilers. *Gaddis et al.*, [1990] report on the use of a mechanical profiler at several points along the December 1974 flow (DEC) on Kilauea Volcano, Hawaii. A 1.8-m horizontal rod which contained 69 freely moving vertical rods, spaced 2.54 cm apart, was used to generate templates of the surface roughness. Five sets of end-to-end measurements were made to generate a 9-m-long profile for each site. Elevations were measured by digitizing photographs of each template in place on the surface, and all profiles were detrended. Vertical accuracy is estimated to be within a few millimeters. Orthogonal measurements along and across flow were made at each of 13 sites, giving a total of 26 profiles. Flow textures range from clinker and ball a'a to spiny, ropy, and slabby pahoehoe.

4.1.3. Line and transit. *Campbell and Garvin* [1993] report on measurements of several basalt flows at Kilauea Volcano (KIL) using a line and transit system. Essentially, a marked line is stretched horizontally along a surface, and a transit at one end is used to measure the height of a stadia rod moved incrementally along the surface. Some later profiles were collected using a laser range finder to improve the horizontal positioning. Profile lengths range from 100 to 120 m with a horizontal interval of 25 cm. Vertical accuracy is estimated to be ±2 cm. A total of 12 sites are considered here. Unlike the data discussed in section 4.1.1, both raw and detrended data can be compared. Flow textures range from rough clinker a'a to an extremely smooth sheet pahoehoe.

J.J. Plaut et al. (manuscript in preparation, 2000) report on measurements of several silicic lava flows at Inyo Domes (ID), California, using a simplified "line and measuring rod" system. Essentially, a measuring rod is moved along a taut rope at regular intervals. Profile lengths are 20 m, with a horizontal spacing of 25 cm. Vertical accuracy is estimated to be ±3 cm. Measurements from five sites are reported here, each with two orthogonal profiles (along and across flow), and all profiles were detrended. Flow textures varied from megablocks to tephra mantled.

4.1.4. Differential global positioning system (GPS). For long baselines of moderate spacing intervals, differential GPS is practical in the field, though not without some inconvenience in analysis. A GPS base station is set up at a

Table 1. Sites Investigated and Roughness Parameters for All Applicable Scales[a]

Name	Note[b]	Description	ξ, cm			θ_{RMS}, deg				H_1	H_2	Breakpoint, cm
			10cm	1m	10m	1 cm	10 cm	1 m	10 m			
DEC 1 (x)	1	ropy pahoehoe	3.5	7.4			34.1	8.2		0.45	0.27	20
DEC 1 (y)	1	ropy pahoehoe	1.6	3.7			16.9	4.4		0.44	0.21	57
DEC 2 (x)	1	sheet pahoehoe	6.1	10.6			48.1	12.2		0.29		
DEC 2 (y)	1	sheet pahoehoe	5.0	8.6			44.0	9.8		0.43	0.18	14
DEC 3 (x)	1	slab pahoehoe	5.6	10.6			46.5	11.6		0.32		
DEC 3 (y)	1	slab pahoehoe	3.7	8.5			36.4	9.7		0.49	0.17	32
DEC 4 (x)	1	spiny pahoehoe	4.0	8.2			37.7	10.4		0.39		
DEC 4 (y)	1	spiny pahoehoe	5.5	11.8			46.0	14.9		0.40		
DEC 5 (x)	1	clinker a'a (85%) 10-50 cm in size	4.8	8.0			42.1	7.1		0.38	0.07	36
DEC 5 (y)	1	and 15% transitional lava plates	6.3	9.3			48.5	7.5		0.26	-0.02	31
DEC 6 (x)	1	ball a'a 30-130 cm in size with	7.9	15.8			57.0	16.2		0.40	0.04	38
DEC 6 (y)	1	some clinker	6.8	16.3			52.6	17.3		0.45	0.14	60
DEC 7 (x)	1	ball a'a (60%) 50-150 cm	7.8	18.7			58.1	18.8		0.55	0.14	34
DEC 7 (y)	1	and clinker (35%) 5-25 cm	9.1	15.7			60.1	14.4		0.40	0.02	27
DEC 8 (x)	1	clinker a'a (65%) 10-70 cm and	7.0	14.4			52.7	17.2		0.38		
DEC 8 (y)	1	ball a'a (35%)	6.8	13.5			53.5	15.0		0.41	0.05	36
DEC 9 (x)	1	clinker a'a (90%) uniform 5-20 cm	6.8	13.5			54.3	15.5		0.55	0.04	22
DEC 9 (y)	1	and ball a'a (10%) 15-30 cm	6.1	10.4			49.5	10.7		0.39	-0.01	21
DEC10 (x)	1	clinker a'a (90%) 10-40 cm and	6.7	11.7			52.6	11.0		0.42	-0.07	22
DEC10 (y)	1	ball a'a (10%) 40-120 cm	6.5	12.6			51.1	13.3		0.35		
DEC11 (x)	1	clinker a'a (85%) 20-50 cm and	5.5	9.8			44.6	10.7		0.32		
DEC11 (y)	1	ball a'a (15%) 30-70 cm	5.8	9.2			46.6	10.0		0.32	0.18	18
DEC12 (x)	1	clinker a'a (85%) 20-50 cm and	7.3	14.0			54.5	13.6		0.38	0.02	39
DEC12 (y)	1	ball a'a (15%) 40-100 cm	6.8	12.8			51.7	14.2		0.31		
DEC13 (x)	1	ball a'a (50%) 30-130 cm and clinker	5.8	9.6			45.4	10.7		0.28		
DEC13 (y)	1	(40%) 5-30 cm, plates (10%)	5.0	8.4			42.5	7.7		0.30	-0.16	57
KIL 1	2	ponded pahoehoe		1.8	6.2			2.2	0.7	0.65	0.07	550
KIL 2	2	ponded pahoehoe with 1m tumuli		4.7	17.7			5.9	2.4	0.69	0.38	500
KIL 3	2	intermediate pahoehoe; tilted plates		10.7	25.3			12.0	3.0	0.40		
KIL 4	2	intermediate billowy pahoehoe		7.9	17.1			9.0	1.9	0.43	0.18	420
KIL 5	2	a'a flow; large, tilted, spiny plates		13.8	24.0			13.5	2.9	0.24	0.40	280
KIL 6	2	intermediate pahoehoe, similar to KIL4		8.4	23.3			10.0	2.8	0.52	0.13	680
KIL 7	2	channelized ropy pahoehoe		13.3	52.4			16.2	7.9	0.68		
KIL 8	2	platy pahoehoe with significant tilts		5.2	11.5			5.7	1.4	0.41	0.07	890
KIL 9	2	a'a flow; mostly small spiny plates		12.5	21.7			12.3	2.3	0.28		
KIL 10	2	sheet pahoehoe flow; ropy structure		5.5	13.9			6.2	1.7	0.48	0.11	820
KIL 11	2	smooth to intermediate pahoehoe		4.1	13.4			5.1	1.9	0.59		
KIL 15	2	very smooth thin-lobed pahoehoe		2.2	5.8			2.7	0.8	0.66	0.41	130
DV12 (x)	3	Devils Golf Course:	3.6	9.8		63.3	41.3	10.2		0.62	0.11	25
DV12 (y)	3	eroded, silty salt	3.5	10.0		62.3	40.9	10.6		0.64	0.32	18
DV15 (x)	3	Trail Canyon alluvial fan:	2.8	4.9		61.8	29.1	5.9		0.52	0.17	7
DV15 (y)	3	intermediate age, active surface	2.5	6.0		57.5	28.3	8.4		0.56	0.29	7
DV18 (x)	3	flood plain surface:	1.5	3.5		42.9	19.3	3.7		0.62	0.37	7

Table 1. (continued)

Name	Note[b]	Description	ξ, cm			θ_{RMS}, deg				H_1	H_2	Breakpoint, cm
			10cm	1m	10m	1 cm	10 cm	1 m	10 m			
DV18 (y)	3	central Death Valley	1.4	3.8		55.5	19.0	4.4		0.31	0.45	3
DV22 (x)	3	Mars Hill, eroded fanglomerate	1.6	4.5		45.6	21.8	7.1		0.50	0.04	103
DV22 (y)	3		1.7	4.2		48.5	23.4	5.4		0.58	0.35	13
DV24 (x)	3	Mars Hill, eroded fanglomerate	2.4	6.5		56.6	30.0	8.5		0.55	0.32	22
DV24 (y)	3		2.0	4.1		53.6	23.6	5.1		0.53	0.32	7
DV25 (x)	3	Mars Hill, eroded fanglomerate	2.4	6.0		53.2	29.5	6.9		0.63	0.33	13
DV25 (y)	3		2.2	5.7		52.6	27.7	6.5		0.53	0.11	36
DV29 (x)	3	active dunes near Stovepipe Wells	1.3	2.9		65.4	19.6	3.9		0.30	0.12	59
DV29 (y)	3		1.0	2.2		36.0	12.3	2.7		0.38		
DV36 (x)	3	Kit Fox alluvial fan:	0.7	1.5		29.8	7.5	2.1		0.51	0.18	3
DV36 (y)	3	young, inactive surface	1.0	2.3		33.4	10.5	2.9		0.60	0.25	3
DV39 (x)	3	Stovepipe Wells alluvial fan at	0.5	0.8		24.0	5.2	0.8		0.42	0.19	3
DV39 (y)	3	east edge of dunes	0.6	0.8		27.9	5.5	1.0		0.34	0.21	1
LC08 (x)	3	older basalt flow with silt	1.6	3.4		52.2	19.6	4.0		0.41	0.18	32
LC08 (y)	3	mantle, northern LCVF	1.4	2.8		45.0	18.2	3.9		0.56	0.36	5
LC11 (x)	3	older basalt flow with silt	1.5	2.6		48.6	17.0	2.5		0.46	0.16	8
LC11 (y)	3	mantle, northern LCVF	1.3	2.4		40.4	16.1	2.6		0.56	0.28	7
LC13 (x)	3	older basalt flow with silt	1.8	4.2		50.3	21.4	5.0		0.43	0.05	67
LC13 (y)	3	mantle, northern LCVF	1.7	3.9		49.6	21.9	4.3		0.48	0.14	27
LC17 (x)	3	Black Rock a'a flow, young	5.6	19.1		73.3	53.8	26.6		0.58		
LC17 (y)	3	northern lobe	4.8	15.0		69.4	48.9	20.1		0.53		
LC23 (x)	3	Black Rock a'a flow, young	4.2	10.5		69.3	43.6	13.3		0.56	0.41	6
LC23 (y)	3	southern lobe	4.0	10.1		65.1	43.0	12.4		0.68	0.38	7
LC25 (x)	3	Black Rock a'a flow, young	4.7	12.6		70.1	47.4	15.6		0.61	0.37	11
LC25 (y)	3	silt-mantled southern lobe	4.6	12.5		67.4	47.9	16.5		0.69	0.42	7
LC27 (x)	3	Black Rock a'a flow, young	3.7	7.7		68.1	39.3	8.0		0.55	0.20	10
LC27 (y)	3	silt-mantled southern lobe	4.3	10.1		67.2	44.5	11.3		0.67	0.36	6
LC29 (x)	3	Black Rock a'a flow, young	3.8	9.0		66.5	40.0	9.7		0.60	0.36	7
LC29 (y)	3	silt-mantled southern lobe	3.9	8.3		66.1	41.1	9.0		0.64	0.29	7
LC39 (x)	3	Lunar Lake Playa, LCVF	0.5	0.7		22.0	4.8	0.7		0.42	0.13	4
LC39 (y)	3	northern end of playa	0.4	0.6		13.7	4.4	0.6		0.59	0.22	5
LC43 (x)	3	Lunar Lake Playa, LCVF	0.7	1.1		28.1	8.3	1.1		0.47	0.12	8
LC43 (y)	3	middle of playa	0.5	0.9		19.2	5.7	0.9		0.49	0.26	7
LC47 (x)	3	Lunar Lake Playa, LCVF	0.4	0.8		13.3	4.9	0.8		0.46	0.10	24
LC47 (y)	3	southern end	0.4	0.9		12.8	4.8	0.9		0.53	0.09	24
LC52 (x)	3	Lunar Lake Playa, LCVF	0.4	1.3		15.6	6.0	1.5		0.55	0.16	46
LC52 (y)	3	model site for GRSFE	0.5	1.3		17.1	6.4	1.5		0.49	0.16	51
LC58 (x)	3	intermediate age basalt flow,	2.3	4.7		67.9	27.6	4.8		0.33	0.02	42
LC58 (y)	3	adjacent to playa, GRSFE model site	2.2	4.0		54.0	25.6	4.1		0.64	0.18	6
LC59 (x)	3	intermediate age basalt flow,	1.8	3.3		47.5	20.7	3.4		0.63	0.21	6
LC59 (y)	3	adjacent to playa, GRSFE model site	1.9	3.4		49.0	21.0	3.5		0.64	0.24	5

Table 1. (continued)

Name	Note[b]	Description	ξ, cm			θ$_{RMS}$, deg				H_1	H_2	Breakpoint, cm
			10cm	1m	10m	1 cm	10 cm	1 m	10 m			
LC60 (x)	3	intermediate age basalt flow,	1.5	2.4		46.2	15.6	2.4		0.54	0.16	5
LC60 (y)	3	adjacent to playa, GRSFE model site	1.6	2.7		47.6	16.9	2.7		0.58	0.22	4
LC65 (x)	3	intermediate age basalt flow	1.4	2.4		45.6	14.7	2.6		0.52	0.23	4
LC65 (y)	3	northeast of Lunar Crater	1.7	2.3		49.7	16.3	2.2		0.59	0.12	4
ID40 (x)	4	Obsidian Dome, vent region with		31.4				33.5		0.52		
ID40 (y)	4	megablocks		50.0				43.9		0.42		
ID180 (x)	4	Wilson Dome, vent region with		8.5				9.0		0.42		
ID180 (y)	4	heavy tephra mantle		11.2				11.6		0.37		
ID210 (x)	4	Obsidian Dome, ridged		30.3				30.0		0.42		
ID210 (y)	4			25.2				25.4		0.38		
ID230 (x)	4	Obsidian Dome, ridged		33.7				34.1		0.47		
ID230 (y)	4			34.4				30.8		0.32		
ID250 (x)	4	Obsidian Dome, jumbled		35.0				35.0		0.53		
ID250 (y)	4			38.9				37.2		0.49	0.04	126
SB1	5	thick, blocky, andesitic flow			126				18.3	0.40		
SB2	5	thick, blocky, andesitic flow			116				11.7	0.47		
SB3	5	thick, blocky, andesitic flow			120				14.5	0.50		
SB4	5	thick, blocky, andesitic flow			165				15.4	0.50		
SB5	5	thick, blocky, andesitic flow			97				7.9	0.29		

a. The parameter ξ is the RMS height at the scale listed; θ_{rms} is the RMS slope at the listed scale; H_1 is the Hurst exponent from the lowest scale up to the smaller of 10% of the profile length or break point; H_2 (if listed) is the Hurst exponent from the breakpoint to 10% of the profile length; and breakpoint (if listed) is the scale at which the Hurst exponent appears to change in the deviogram. Uncertainties in our estimates of RMS height are approximately ±1 mm for DEC, KIL, DV, and LC sites; ±5 mm for ID and SB sites (see sections 4.1 and 4.2 for uncertainty in individual measurements or the notes). Uncertainties in RMS slope vary with scale; at the centimeter scale they are ±10°; at 10 cm and higher scales they are ±1° or less. Uncertainties in the Hurst exponents are ±0.05 or less. Uncertainties in the breakpoints are estimated to be ±20%.

b. Notes: (1) Kilauea, Hawaii, December 1974 flow; sample technique, mechanical profiler; profile length 9 m; sample interval 2.5 cm; vertical uncertainties ±5 mm. *x* and *y* are perpendicular profiles; data detrended, largest removed slope 0.1° [*Gaddis et al.*, 1990]. (2) Various flows on Kilauea, Hawaii; sample technique, rope and transit; profile lengths ~100-120 m; sample interval 25 cm; vertical uncertainties are ±1 cm; data detrended, largest removed slope 3.4° [*Campbell and Garvin*, 1993; *Campbell and Shepard*, 1996]. (3) Various surfaces throughout southern California and Nevada; sample technique, helicopter stereophotography; profile lengths *x* 20 m, *y*, (perpendicular to *x*) 10 m; sample interval 1 cm; vertical uncertainties ±3 mm; composite parameters for *x*, five profiles of 20 m and *y*, 10 profiles of 10 m; data detrended, unknown slopes (helicopter was tilted an unknown amount in flight) [*Farr*, 1992; *Arvidson et al.*, 1991]. (4) Inyo Domes, California; sample technique, rope and measuring rod; profile lengths 20 m; sample interval 25 cm; vertical uncertainties ±3 cm; *x* and *y* perpendicular profiles; data detrended (ID40x, 12.4°; ID40y, 15.0°; ID180x, 7.2°; ID180y, 3.8°; ID210x, 10.8°; ID210y, 1.0°, ID230x, 5.3°; ID230y, 4.2°; ID250x, 0.4°; ID250y, 13.4°) [*Anderson et al.*, 1998; *Plaut et al.*, 2000, manuscript in preparation]. (5) Sabancaya volcano, Peru; sample technique, differential GPS; profile lengths, 400-1300 m; sample interval, ~3 m; vertical uncertainties ±2 cm; data detrended (slopes SB1, 2.0°; SB2, 0.6°, SB3 4.0°, SB4 6.8°, SB5, 2.9°) [*Bulmer and Campbell*, 1999; *Bulmer et al.*, 1999].

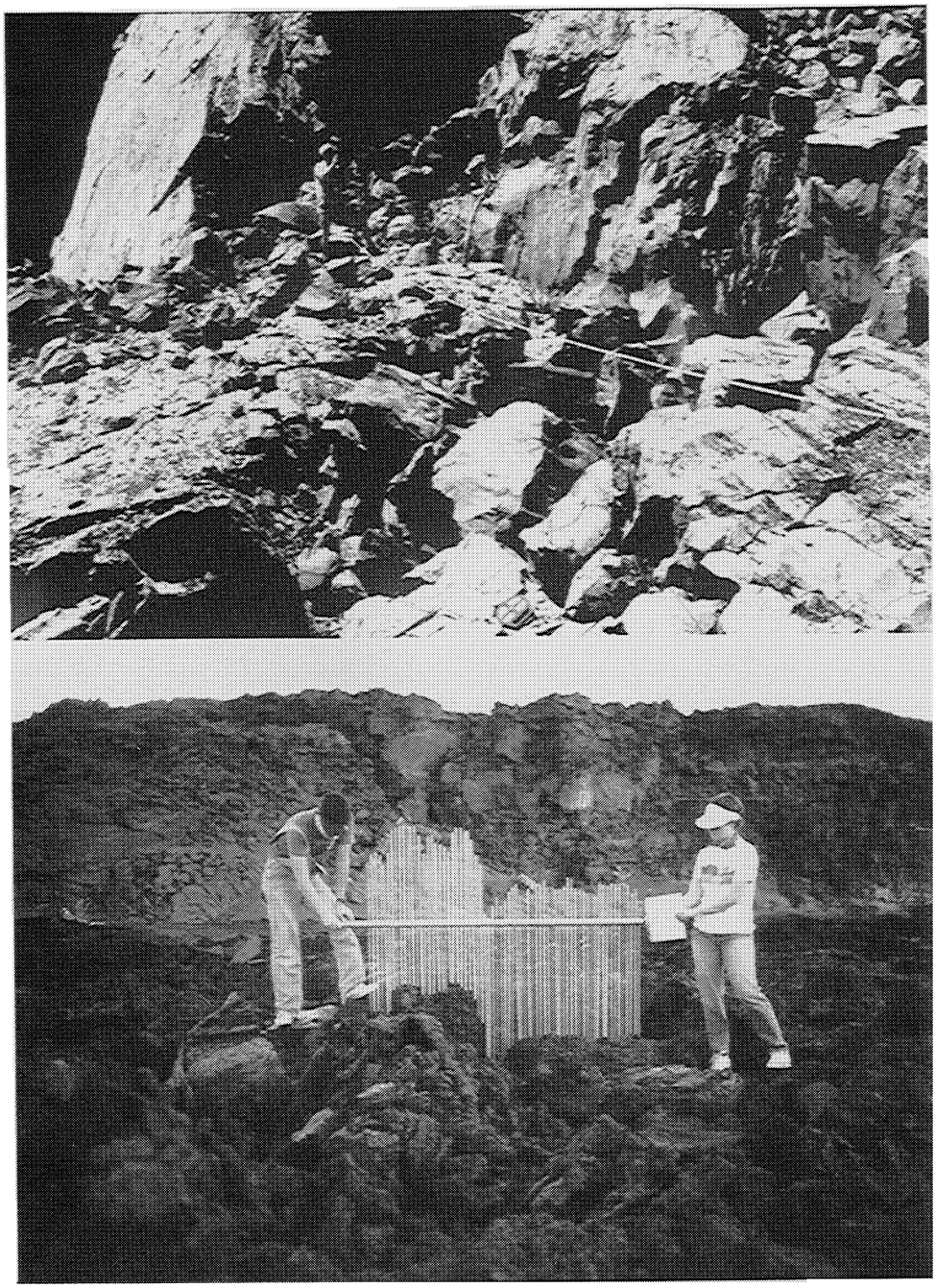

Figure 5. Photographs of several sites examined in this study. (a). Rhyolitic flow in the Inyo Domes (ID40). One of the roughest sites in our survey. A standing person is visible in the upper left for scale. (b) Rough a'a flow displaying lava balls, clinker, and plates on the December 1974 flow, Kilauea, Hawaii. (DEC6) (c) Ponded pahoehoe flow at Kilauea showing small, glassy weathered fragments(KIL1). (d) Lunar Lake Playa, Nevada (LC39). The strong Sunglint from the surface emphasizes its smooth nature. Vegetation is ~1 m in height. (e) Helicopter view of the Devils Golf Course (DV12), an eroded salt surface made up of jagged pinnacles which exhibits isotropic roughness behavior. The image is ~30 m x 30 m. (f) Helicopter view of Kit Fox alluvial fan (DV36). This is a young, inactive surface composed of easily eroded pebbles and cobbles. The directional nature of the channel causes anisotropic roughness behavior. The image is ~30 m x 30 m, and the shadow of the helicopter is visible at the bottom of the photograph.

site and another GPS unit, linked to the base station, is moved along the transect. Horizontal and vertical uncertainties are ±2 cm. One difficulty with this method is that the horizontal spacing between sample points is often not uniform and introduces some scatter in the analysis. *Bulmer and Campbell* [1999] made measurements along several transects of an andesitic flow from the Sabancaya stratovolcano (SB) in Peru. Profile lengths are of the order of 400-1300 m with a mean horizontal spacing interval of ~3 m. The flow texture is uniformly blocky.

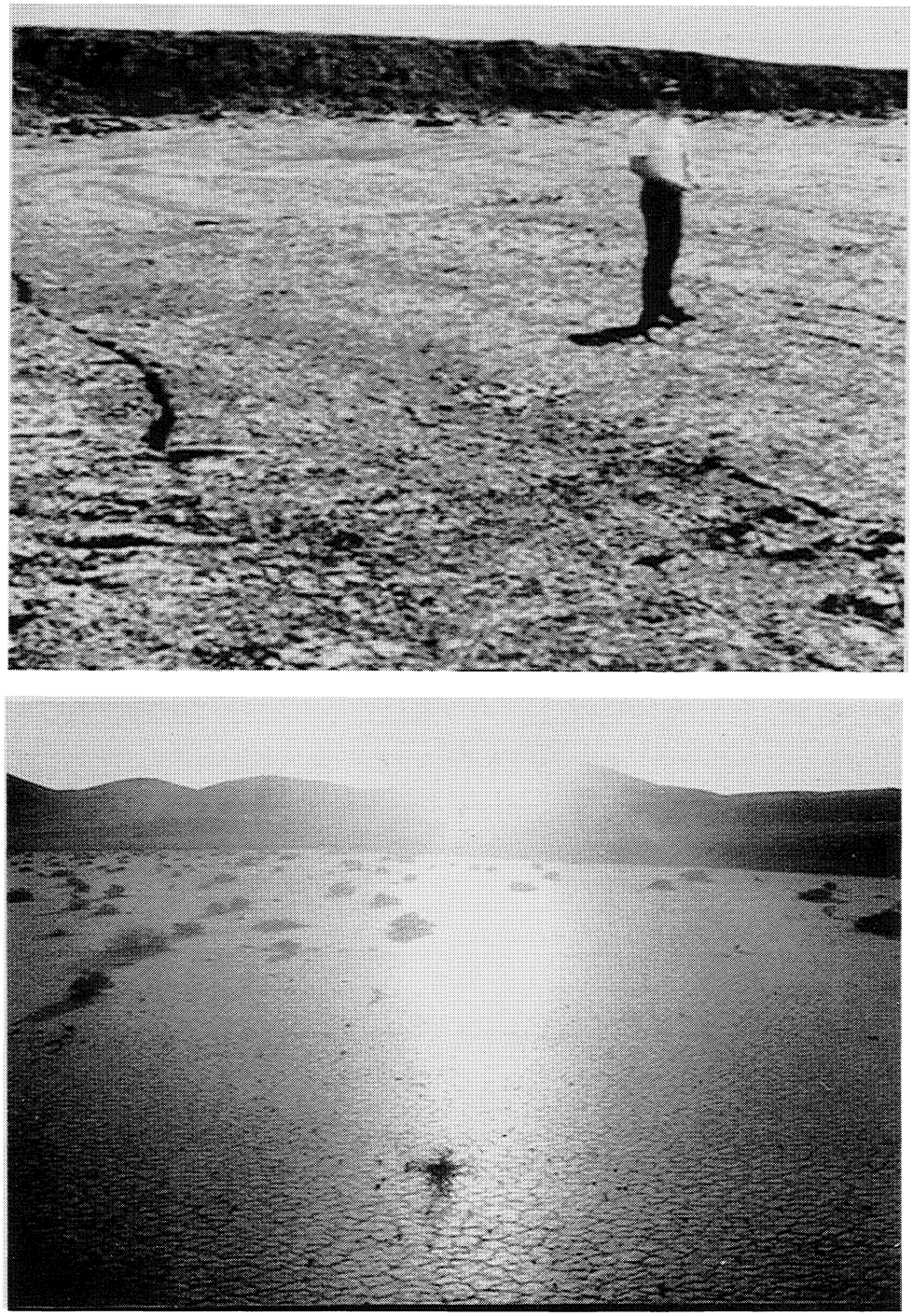

Figure 5. (continued)

4.2. Results of Analysis

The parameters for each profile reported in Table 1 include the RMS height and RMS slope at all applicable powers of 10, and Hurst exponent, H_1, from the smallest scale up to one-tenth of the profile length, or until a significant change is observed. In this latter case, a new Hurst exponent, H_2, is measured and the scale at which the transition occurs, or breakpoint, is reported.

4.2.1. Comparison of roughness at similar scales. One of the most powerful outcomes of our standardization is that measures like the RMS height or slope of different surfaces measured by different workers with different tools can be meaningfully compared at similar scales. For example, compare the RMS height at the 1-m scale for pahoehoe flows measured along the Kilauea December 1974 flow (DEC) [*Gaddis et al.*, 1990], and those measured by *Campbell and Garvin* [1993] at a variety of Kilauea locations (KIL). The DEC flows range from 3.7 to 11.8 cm; the KIL flows range from 1.8 to 13.3 cm. A'a flows from these sites can also be compared with those measured by *Farr* [1992] (LC17–LC29).

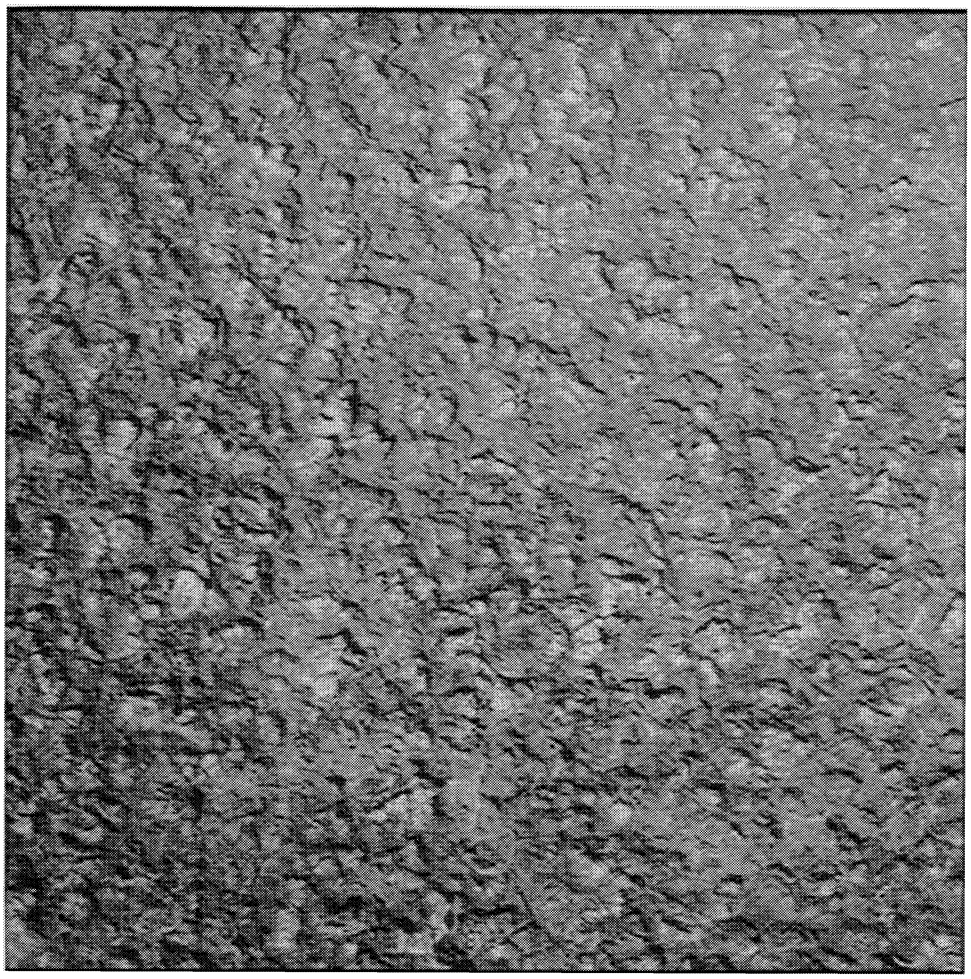

Figure 5. (continued)

For the DEC flows the RMS height at 1 m range from 8.0 to 18.7 cm; the KIL flows (only two) range from 12.5 to 13.8 cm; the LC flows range from 7.7 to 19.1 cm. Despite the fact that all of these were measured by different workers with radically different tools, the roughness statistics are consistent with one another as one would expect from similar terrain. In contrast, the 1-m-scale RMS height of four of the five silicic flows (all but ID180) at Inyo Domes (J.J. Plaut et al. manuscript in preparation, 2000) range from 25.2 to 50.0 cm, and for several sites on the Lunar Lake playa (LC39-LC52) from 0.6 to 1.3 cm. Thus by standardizing the scale at which statistics are reported, intrinsic roughness differences are emphasized.

4.2.2. Extremes in surface roughness. Now that we have a means for comparing the roughness of surfaces, it becomes inevitable that we look for the extremes in roughness behavior. Figure 5 shows photographs of several sites in our data sets; Figures 5a-5d span the total range of surface roughness encountered. The roughest by far is the Inyo Dome flow ID40 with an RMS height of 50 cm at the 1-m scale and RMS slope of 44° at 1-m steps (Figure 5a). For comparison, one of the roughest basaltic flows (DEC6) has an RMS height of 16 cm and RMS slope of 17° at the same scale (Figure 5b). Figure 5c illustrates one of the smoother pahoehoe flows (KIL1), which has an RMS height and slope of 2 cm and 2°, respectively, at the meter scale. Figure 5d shows the smoothest surface that we examined, the Lunar Lake playa (LC39), with RMS heights and slopes of only 0.6 cm and 0.6° at the meter scale.

A low Hurst exponent indicates that a surface gets smooth rapidly as the scale increases. Although it may be rough at small scales, it appears smooth at large scales. A flat lawn or golf green is a good example. At the millimeter to centimeter scale, blades of grass make a rugged terrain, while at scales of a few meters and above, the surface is quite smooth. The lowest Hurst exponent measured from the smallest scale up is 0.20 for the Stovepipe Wells alluvial fan (DV39). For Hurst exponents after a breakpoint, the lowest values approach 0.0 for some surfaces. This suggests that above the scale of the breakpoint, these surfaces become monotonous statistical copies of themselves; either gravity or erosion has reduced or removed any larger-scale features if they ever existed. Only at these scales can the surface be considered "stationary." Negative Hurst exponents after the breakpoint are observed but rare. Often these are at or near the 10%-of-the-profile-length limit suggested here and indicate poor sampling statistics. However, this may also indicate periodic behavior in the surface with a wavelength of the order of the breakpoint scale.

A large Hurst exponent implies that a surface tends to maintain its roughness as the scale increases. At the limit of $H = 1$, the surface is said to be self-similar and equally rough (or

Figure 5. (continued)

smooth) at any scale measured. Two KIL sites (2 and 7) approach Hurst exponents of 0.7. At site 2, this behavior breaks at a scale of ~5 m, corresponding to the spacing of raised bulges on the lava surface. At site 7, however, the behavior persists up to ~12 m, consistent with the more random a'a texture.

4.2.3. Isotropic and anisotropic behavior. A common assumption in surface roughness models is that the roughness is isotropic, i.e., has no directional dependence. The helicopter stereo data and the DEC and ID profile data were acquired in orthogonal directions, allowing us to test this assumption. Where we have multiple parallel profiles across the same surface (as with the helicopter stereo data), we can average the deviograms of each parallel profile to generate a better overall deviogram for the surface in that direction.

A strictly isotropic surface should display nearly identical deviograms in orthogonal directions (Figures 5e and 6a). From a practical standpoint, one would likely accept an isotropic claim if the roughness in orthogonal directions differed by less than some threshold, 10% being a reasonable starting value. Our investigation reveals that this only occurs in about half of our study sites. Figures 6b-6d illustrate some of the other commonly observed deviogram behaviors. Figure 6b shows the deviogram of a surface with similar scaling behavior (Hurst exponents) in orthogonal directions but significantly different surface roughness (see also Figure 5f). Figures 6c and 6d show deviograms of surfaces with similar roughness at small and large scales, respectively, but with different Hurst exponents. The greatest ratio of orthogonal roughness in this data set, ~3, occurs at the centimeter scale of DV29, a dune field. However, the greatest absolute difference in roughness can be found in the Inyo Domes profiles, ID40, where the RMS heights at the 1-m scale differ by more ~20 cm in perpendicular direction. (On this latter site, however, the difference may reflect a sampling bias caused by undersampling very large scale surface roughness.)

A major cause of anisotropic roughness is directional formation and/or modification processes. Lava flows downslope, and the topography often reflects this directional motion. Alluvial fans form from fluvial processes, again downslope. Eolian structures, like dunes, form in a highly directional wind environment. On much larger scales, tectonic processes are also directional. With so many directional geologic processes, it is somewhat surprising that any surfaces are isotropic. Again, however, we come back to the issue of scale. At the meter to tens of meter scales, we do not "see" the directional nature of tectonic forces. In situ chemical erosion or nondirectional mechanical erosion (e.g., spallation) will homogenize many surfaces at the centimeter scale while leaving the larger scales anisotropic. The rate at which a

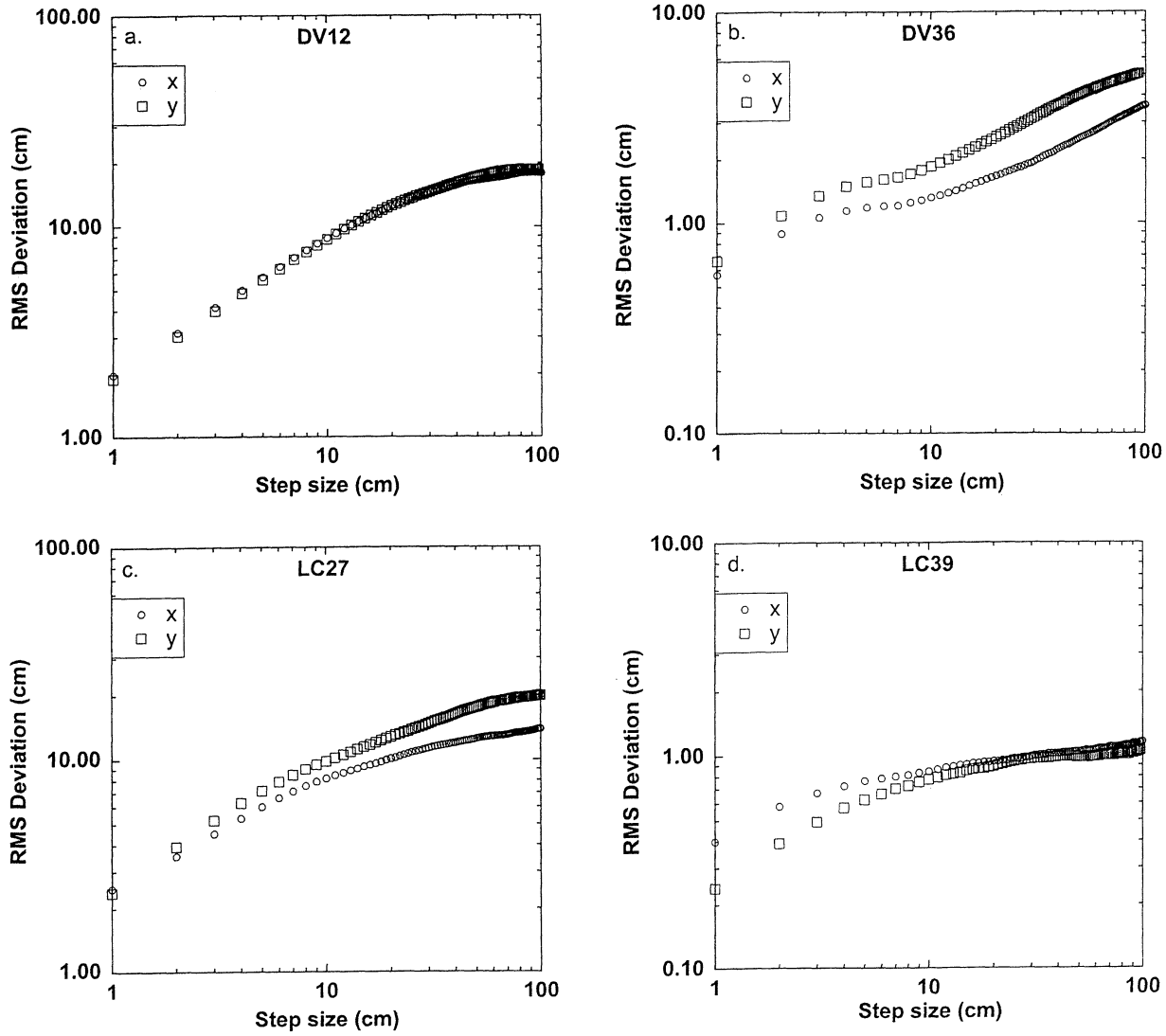

Figure 6. Deviograms illustrating different behaviors in orthogonal directions. (a) Deviograms of similar roughness and scaling behavior, indicating isotropic behavior (DV12, see Figure 5e). (b) Deviograms of similar scaling behavior, but different roughness (DV36, see Figure 5f). (c) Deviograms similar in roughness at small scales but differing at larger scales (silt-covered portion of the Black Rock a'a flow, DV27). (d) Deviograms differing in roughness at small scales but similar at large scales (Lunar Lake playa, LC39).

process occurs often influences the surface roughness and isotropy. At relatively low basalt flow rates, pahoehoe textures form. These are highly directional at the tens of centimeters scale but tend to be more isotropic as scale increases. As the flow rates increase beyond some threshold, whether because of slope steepness or an increase in effusion, the more rugged and randomized a'a flow textures form [*Rowland and Walker*, 1990].

4.2.4. Correlations of Hurst exponent with terrain type. An examination of Table 1 is sufficient to note that there are no obvious correlations between the Hurst exponent and the type of terrain. In fact, as demonstrated in section 4.2.3, the Hurst exponent can differ significantly on the same surface in different directions. We conclude that different geological surfaces cannot be reliably distinguished from one another on the basis of their scaling behavior alone. Figure 7 shows a histogram of all measured Hurst exponents, which cluster between 0.2 and 0.7 for the surfaces; the vast majority occur between 0.4 and 0.6. Surfaces with Hurst exponents of 0.5 are termed "Brownian" since Brownian motion will produce a random surface of this type [cf. *Turcotte*, 1997], and others have noted the strong tendency for natural surfaces to cluster around this behavior [*Sayles and Thomas*, 1978].

4.2.5. Relationship of breakpoints to surface expression. It has been hypothesized that the breakpoints may be related to differences in the scale of surface features or processes [*Campbell and Shepard*, 1996], and the data examined here support that hypothesis. The Lunar Lake Playa (LC39,43,47,52) is covered with desiccated polygonal cracks that vary in size from place to place. The physical size of these polygons range from a few centimeters to several tens of centimeters, consistent with the location of the breakpoints for each deviogram. The December 1974 flow (DEC) sites 5 to 13 were all variations of a'a, consisting primarily of clinkers and

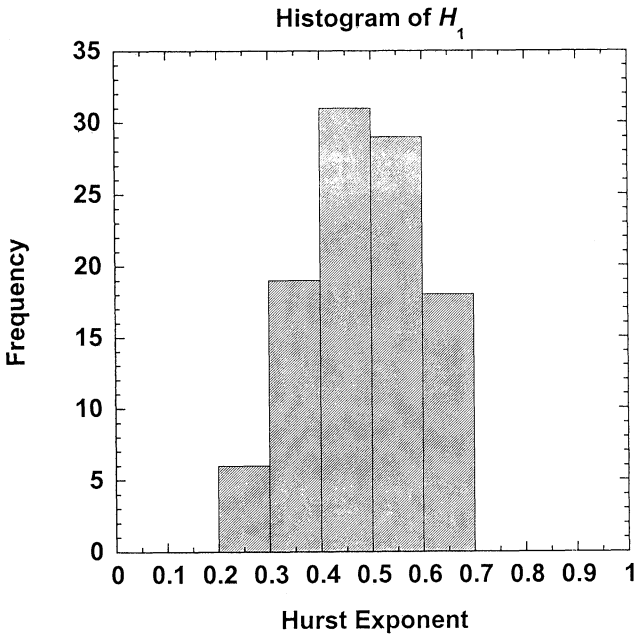

Figure 7. Histogram of Hurst exponents observed in these data (only H_1). Note the tendency to cluster around $H = 0.5$, also referred to as "Brownian" behavior.

ball lava. The dimensions of these features ranged from 5 to 150 cm, depending upon the flow [*Gaddis et al.*, 1990], consistent with the scale of the breakpoints listed in Table 1. Mars Hill is an eroded fanglomerate famed for its visual similarity to the surface of Mars near the Viking landing sites. For the deviograms of this site that display breakpoints, values range from ~20 to 50 cm, again consistent with measured larger rock sizes [*Golombek and Rapp*, 1995]. The deviograms of the Inyo Domes generally do not display breakpoints up to the 2-m scale (limit), consistent with the observation that the larger blocks exceed this size [*Anderson et al.*, 1998].

5. Application to Planetary Surfaces

5.1. Planetary Surface Measurements

The number of planetary surfaces for which surface roughness data are available is quite small. Landers have set down at a number of Venus sites, but to our knowledge, none of these sites have been quantitatively characterized for surface roughness. The two Viking landing sites were exhaustively studied by a number of investigators, including those who determined the size-frequency distribution of rocks [*Golombek and Rapp*, 1995; *Moore and Keller*, 1990]. However, none extracted estimates of surface roughness compatible with those discussed here. A digital elevation model for the Mars Pathfinder landing site was studied by *Haldemann et al.* [1997] using some of the techniques advocated here. They found that the surface was approximately Brownian over the scales of measurement (a few centimeters to several meters). Data on lunar surface roughness are equally sparse at these scales. *Helfenstein and Shepard* [1999] analyzed microscale topography using photographs from the Apollo Lunar Surface Closeup Camera (ALSCC). The scales of that investigation ranged from ~0.9 mm to ~9 cm; the Hurst exponent ranged from 0.5 to 0.6 and the RMS slope ranged from 12° to 37° at the millimeter scale.

5.2. Lander Safety Issues

The surface of Mars is fairly rough at the meter scale as observed by the Viking Landers, Pathfinder mission, and Mars Orbiter Camera. A "typical" soft lander is of the order of 3 m across, and the landing safety criteria for such a lander (using the now cancelled Mars Surveyor 2001 Lander as a representative) are (1) <1% chance of landing on a protrusion (rock) of >33 cm height and (2) no surface slopes (at lander scales) of >10° [*Golombek et al.*, 1999]. We can restate these requirements as an approximately Gaussian surface whose RMS height is <11.0 cm and RMS slope <3.3° at a horizontal scale of 3 m. Of the data sets described here, two are well suited for examining surface roughness at lander scales. The Hawaiian (KIL) profiles are long enough to provide meaningful statistics at the 3-m scale, and both the raw and detrended profiles are available for examination. The helicopter stereo-derived profiles include three areas from the Mars Hill site in Death Valley, California. Mars Hill, a good visual analog for the Viking landing sites, is an informally named, low rounded sandy hill, devoid of vegetation, and scattered with wind-polished basaltic boulders. The Mars Hill sites, however, can only be tested for the RMS height criterion; the unknown slope of the helicopter in flight (removed during detrending) makes it impossible to determine true ground slopes.

Rather than measure the RMS height at scales of 3 m, we found the maximum height within all possible 3-m profiles (using the endpoints of the profile as the zero baseline, just like a lander) and the total fraction of the profile that would exceed the 33 cm height threshold. Of the 12 Hawaiian sites, nine had local spots that exceeded the threshold, and of these, eight exceeded the threshold over more than 1% of their length. The roughest of these was KIL5, an a'a flow, which has a maximum height of 71 cm and exceeds the threshold over 23% of its length. The three Mars Hill sites, while a good visual analog, are generally rougher than the observed landing sites on Mars [*Golombek and Rapp*, 1995]. Of the 45 available profiles, 18 exceeded the 33-cm threshold over more than 1% of the profile. The roughest of these had a maximum height of >80 cm. Nine of the 12 Hawaiian profiles exceeded the maximum RMS slope threshold of 10°. All of these profiles are approximately Gaussian at these scales, so their RMS slope is a good estimator of the statistical width of the distribution. Of these, KIL7 was by far the roughest, with an RMS slope of 12° at the 3-m scale, and a maximum slope of 36°. This type of evaluation in other Mars analog terrains could aid scientists and engineers in designing landers and choosing appropriate sites.

5.3. Remote Sensing Applications

5.3.1. Interpreting scale and anisotropic roughness. The vast majority of our information about other planets comes from remote observations. Most of the remote-sensing models in use by the optical, thermal, and radar communities include some type of correction for or extraction of surface roughness.

Until recently, however, most of these models have relied upon single-parameter roughness measures, often assuming that the surface roughness could be modeled as a stationary process. Because of this, the physical meaning of roughness parameters extracted from these models is inherently ambiguous with regard to scale and of limited use in comparative planetology. Some progress has been made recently in the microwave regime to incorporate scale-dependent roughness models [*Shepard and Campbell*, 1999; *Campbell and Shepard*, 1996; *van Zyl et al.*, 1991], and efforts are underway to make similar progress in the optical and thermal regimes. However, any roughness parameters extracted from such models must be compared to those of terrestrial counterparts before a real "geologic" sense of the surface roughness can be obtained. One important finding from this study is that many surfaces have anisotropic roughness. They will appear differently depending upon the direction from which they are illuminated and viewed, and a single roughness characterization, even using scale-dependent statistics as advocated here, may be misleading. This confirms and extends similar findings by *Gaddis et al.* [1990].

5.3.2. Variation of surface roughness with incident wavelength. The topographic data presented here are highly relevant to an understanding of radar scattering, which is usually confined to scales between 3 cm (X band) and ~70 cm (P band). Our current understanding of the radar scattering process is that wavelength-scale roughness dominates the so-called "diffuse" component of the echo [*Hagfors*, 1967; *Campbell and Shepard*, 1996]. Recent work also suggests that wavelength-scaled roughness and the Hurst exponent are important parameters controlling the "quasi-specular" echo [*Shepard and Campbell*, 1999]. The data presented here illustrate that surface roughness differs depending on the scale at which it is measured. Using the methods illustrated here, we can directly calculate from the data (or estimate from Equations (6) and (9)) the RMS height and slope of a surface at different radar wavelengths. For example, the RMS height of the Mars Hill fanglomerate (DV22x) is 1.8 cm, 2.5 cm, and 4.3 cm at S (12 cm), L (24 cm), and P (70 cm) wavelengths, respectively; the equivalent RMS slopes are 20.0°, 14.2°, and 8.3°, respectively.

An interesting prospect arises if a surface is examined in multiple wavelengths. Assuming that the roughness at the various wavelength scales can be extracted using a suitable model, an estimate of the scaling behavior (Hurst exponent) can be made. *Campbell and Shepard* [1996] demonstrated this using AIRSAR C (6 cm), L (24 cm), and P (68 cm) band data obtained at the KIL sites reported here. This kind of analysis could potentially even extend across traditional wavelength boundaries; for example, optical, thermal, and microwave studies of the same region could characterize the roughness state from micrometers to meters.

5.3.3. Interpolating backscatter cross sections between radar wavelengths. When comparing radar backscatter cross-sections of terrestrial sites imaged with synthetic aperture radar (SAR) systems to those used by planetary orbiters (e.g., Magellan), we are often confronted with comparing cross-sections measured at different wavelengths. For example, the Airborne SAR (AIRSAR) system measures cross sections at C (6 cm), L (24 cm), and P (68 cm) bands, while Magellan used an S band (12 cm) system [*van Zyl et al.*, 1991; *Tyler et al.*, 1991]. Given backscatter cross sections at C and L bands for a particular terrestrial site, it is common practice to interpolate between the two to synthesize an equivalent S band cross section for direct comparison with Magellan observations [e.g., *Arvidson et al.*, 1992; *Campbell and Campbell*, 1992]. The most common method employed is to weight the interpolation by wavelength, so that the C band component receives roughly twice the weight of the L band component. However, if the surface topography is self-affine over the range of horizontal scales applicable to radar scattering, then the echo strength may scale in a similar manner. This has been demonstrated for the depolarized (or cross-polarized) echo by *Campbell and Shepard* [1996] and may be applicable for other polarization states as well. Given the backscatter cross-section, σ^o, at some wavelength, λ_1, a self-affine relationship predicts that

$$\sigma^o(\lambda_2) = \sigma^o(\lambda_1)\left[\frac{\lambda_1}{\lambda_2}\right]^H. \quad (10)$$

An interesting consequence of (10) is that the backscatter cross section interpolated between values at two wavelengths is independent of the Hurst exponent, H. For example, a simulated S band (12 cm) echo, in dB, from AIRSAR C and L band data is given by

$$\sigma^o_{dB}(12\,\text{cm}) = 0.5\sigma^o_{dB}(6\,\text{cm}) + 0.5\sigma^o_{dB}(24\,\text{cm}). \quad (11)$$

Thus, if a surface is self-affine, an average of the C and L band echo would be a better estimate of the S band echo than interpolation based upon wavelength.

5.3.4. Optimum radar wavelengths for a given surface roughness. With some a priori knowledge of the terrain roughness, one can select an optimum wavelength (or range of wavelengths) with which to study a surface remotely. There is evidence [*Campbell and Shepard*, 1996] that the radar backscatter cross section saturates when the (projected) RMS slope of the surface at the wavelength scale exceeds 45°, or the (projected) RMS height exceeds $\lambda/4$ (the Rayleigh criterion). Because these criteria are projected roughness values, even a "rough" surface can appear smooth if illuminated near grazing incidence. Using this as an approximate guide, a radar system will be most effective for discriminating variations in surface roughness when

$$\xi_\lambda \le \frac{\lambda}{4}\cos\theta \quad \text{or} \quad s_\lambda \le \cos\theta, \quad (12)$$

where the ξ_λ and s_λ are the RMS height and slope, respectively, of a surface measured at a scale of one wavelength, and θ is the illumination or incidence angle. As an example, an S band system (12 cm) illuminating a surface at θ= 45° would discriminate among surfaces with RMS heights of ≤4.2 cm and RMS slopes of ≤ 54° at the 12 cm scale. Using (6) and (9) and assuming Brownian behavior (H = 0.5), this corresponds to ξ(10 cm) ≤ 3.8cm and/or θ_{rms}(10

cm) ≤ 56°. A review of Table 1 shows that roughly half of the applicable (those for which we have 10-cm scale data) surfaces meet this criterion. A similar analysis for P band (70 cm) shows that the majority of surfaces meet the criteria of (12). However, while P band may be theoretically capable of a broader range of surface roughness discrimination than S band, it would have greater difficulty with very smooth surfaces because some level of apparent surface roughness is necessary to generate a measurable echo. On the basis of the results of *Campbell and Shepard* [1996] (which are for cross-polarized echoes, HV), a surface should have a wavelength-scaled RMS height of at least a few percent of the wavelength, or RMS slope of ~5° or more at the wavelength scale to be detectable.

6. Conclusions

We suggest reporting (1) the length and step interval of topographic data, (2) whether detrending occurred and, if so, the slope removed, (3) RMS height at power-of-ten scales, (4) RMS slope or deviation at power-of-ten scales, (5) the scaling behavior of the surface roughness as quantified by the Hurst exponent and, if applicable, its breakpoint(s), and (6) uncertainties in measurements and the reported parameters above. As demonstrated here, these properties provide a means of comparing data sets gathered by workers using different measurement methods. They should also be of use for any instrument design or modeling in which surface roughness plays a role; examples discussed here include the development of remote-sensing models, design of remote sensors for specific terrain types, and planetary lander design and site selection.

We have found that most surfaces exhibit roughness scaling behavior consistent with Brownian noise ($H = 0.5$), although significant deviations from this are found. We found that different geologic surfaces could not be distinguished from one another using their scaling behavior (Hurst exponent) alone. There does, however, appear to be a correlation between the scale at which a breakpoint in the Hurst exponent occurs and the physical size of topographic features, e.g., mudcracks, lava billows, largest rock diameters. This observation lends support to the hypothesis that breakpoints are related to the different scales at which various processes build and modify surfaces [*Campbell and Shepard*, 1996]. Roughly half of the surfaces examined displayed significant anisotropic behavior, although this result depends upon the scale in question.

Acknowledgments. M.K.S., B.A.C., L.R.G., and J.J.P. gratefully acknowledge the support of NASA Planetary Geology and Geophysics during this work. M. H. B. was supported by NASA grant NAG5-9000 Solid Earth and Natural Hazards. Part of the work done by T. G. F. was under contract to NASA. The authors thank P. Helfenstein for his review.

References

Anderson, S. W., E. R. Stofan, J.J. Plaut and D. A. Crown, Block size distributions on silicic lava flows surfaces: Implications for emplacement conditions, *Geol. Soc. Am. Bull., 110*, 1258-1267, 1998.

Arvidson, R. E., M. A. Dale-Bannister, E. A. Guinness, S. H. Slavney, and T. C. Stein, Archive of geologic remote sensing field experiment data, Release 1.0, NASA Planet. Data Syst., Jet Propul. Lab., Pasadena, Calif., 1991.

Austin, R. T., A. W. England, and G. H. Wakefield, Special problems in the estimation of power-law spectra as applied to topographical modeling, *IEEE Trans. Geosci. Remote Sens., GE-32,* 928-939, 1994.

Bulmer, M. H., and B. A. Campbell, Topographic data for a silicic lava flow – A planetary analog, *Lunar Planet. Sci. Conf.* [CD-ROM], *XXX*, Abstract 1446, 1999.

Bulmer, M.H., F. C. Engle, and A. Johnston, Analysis of Sabancaya volcano, southern Peru using RADARSAT and Landsat TM data, paper presented at Application Development Research Opportunity RADARSAT Final Symposium, Can. Space Agency, Montreal, 1999.

Campbell, B. A., and D. B. Campbell, Analysis of volcanic surface morphology on Venus from comparison of Arecibo, Magellan, and terrestrial airborne radar data, *J. Geophys. Res., 97*, 16,293-16,314, 1992.

Campbell, B. A., and J. B. Garvin, Lava flow topographic measurements for radar data interpretation, *Geophys. Res. Lett., 20*, 831-834, 1993.

Campbell, B. A., and M. K. Shepard, Lava flow surface roughness and depolarized radar scattering, *J. Geophys. Res., 101*, 18,941-18,951, 1996.

Chase, C. G., Fluvial landsculpting and the fractal dimension of topography, *Geomorphology, 5*, 39-57, 1992.

Farr, T. G., Microtopographic evolution of lava flows at Cima Volcanic Field, Mojave Desert, California, *J. Geophys. Res., 97*, 15,171-15,179, 1992.

Gaddis, L. R., P. J. Mouginis-Mark, and J. N. Hayashi, Lava flow surface textures: SIR-B radar image texture, field observations, and terrain measurements, *Photogramm. Eng. Remote Sens., 56*, 211-224, 1990.

Golombek, M. and D. Rapp, Size-frequency distribution of rocks on Mars (abstract), in Mars Pathfinder Landing Workshop II: Characteristics of the Ares Vallis Region and Field Trips in the Channeled Scabland, Washington, LPI Tech. Rep. 95-01, 13-15, 1995.

Golombek, M., N. Bridges, M. Gilmore, A. Haldemann, T. Parker, R. Saunders, D. Spencer, J. Smith, and C. Weitz, Preliminary constraints and approach for selecting the Mars Surveyor '01 landing site, *Lunar Planet. Sci. Conf.* [CD-ROM], *XXX*, Abstract 1383, 1999.

Hagfors, T., A study of the depolarization of lunar radar echoes, *Radio Sci., 2*, 445-465, 1967.

Haldemann, A. F. C., R. F. Jurgens, M. A. Slade, and M. P. Golombek, Mars Pathfinder landing site radar properties, *Eos. Trans. AGU 78* (46), Fall Meet. Suppl., F404, 1997.

Helfenstein, P., and M. K. Shepard, Submillimeter-scale topography of the lunar regolith, *Icarus, 141*, 107-131, 1999.

Howard, A. D. and R. A. Craddock, Simulation of erosion of ancient cratered terrain on Mars *Lunar Planet. Sci. Conf.* [CD-ROM], *XXIX*, Abstract 1323, 1998.

Kreslavsky, M. A., and J. W. Head III, Kilometer-scale slopes on Mars and their correlation with geologic units: Initial results from Mars Orbiter Laster Altimeter (MOLA) data, *J. Geophys. Res., 104*, 21,911-21,924, 1999.

Luo, W., R. E. Arvidson, M. Sultan, R. Becker, M. K. Crombie, N. Sturchio, and Z. El Alfy, Groundwater sapping processes, Western Desert, Egypt, *Geol. Soc. Am. Bull., 109*, 43-62, 1997.

Mandelbrot, B. B., *The Fractal Geometry of Nature*, W. H. Freeman, New York, 1982.

Miller, L. S., and C. L. Parsons, Rough surface scattering results based on bandpass autocorrelation forms, *IEEE Trans. Geosci. Remote Sens., 28*, 1017-1021, 1990.

Moore, H. J., and J. M. Keller, Surface material maps of the Viking landing sites on Mars (abstract), in *Reports of Planetary Geology and Geophysics Program - 1989, NASA Tech. Memo., 4210*, 533-535, 1990.

Plaut, J. J., and R. E. Arvidson, Comparison of Goldstone and Magellan radar data in the equatorial plains of Venus, *J. Geophys. Res., 97*, 16,279-16,292, 1992.

Rowland, S. K., and G. P. L. Walker, Pahoehoe and aa in Hawaii: Volumetric flow rate controls the lava structure, *Bull. Volcanol., 52*, 615, 1990.

Sayles, R. S., and T. R. Thomas, Surface topography as a non-stationary random process, *Nature, 271*, 431-434, 1978.

Shepard, M. K. and B. A. Campbell, Radar scattering from a self-affine fractal surface: Near-nadir regime, *Icarus*, *141*, 156-171, 1999.

Shepard, M. K., R. A. Brackett, and R. E. Arvidson, Self-affine (fractal) topography: Surface parameterization and radar scattering, *J. Geophys. Res., 100*, 11,709-11,718, 1995.

Turcotte, D. L., *Fractals and Chaos in Geology and Geophysics*, 2nd ed., Cambridge Univ. Press, New York, 1997.

Tyler, G. L, P. G. Ford, D. B. Campbell, C. Elachi, G. H. Pettengill, and R. A. Simpson, Magellan: Electrical and physical properties of Venus' surface, *Science*, *252*, 265-270, 1991.

van Zyl, J. J., C. F. Burnette, and T. G. Farr, Inference of surface power spectra from inversion of multifrequency polarimetric radar data, *Geophys. Res. Lett.*, *18*, 1787-1790, 1991.

Wall, S. D.,T. G. Farr, J.-P. Muller, P. Lewis, and F. W. Leberl, Measurement of surface microtopography, *Photogramm. Eng. Rem. Sens., 57*, 1075-1078, 1991.

M. K. Shepard, Department of Geography and Geosciences, 400 E. Second St., Bloomsburg University, Bloomsburg, PA 17815, USA. (mshepard@bloomu.edu)

M. H. Bulmer and B. A. Campbell, Center for Earth and Planetary Studies, National Air and Space Museum, Washington, D.C., 20560, USA.

T. G. Farr, MS 300-233 Jet Propulsion Laboratory, 4800 Oak Grove, Pasadena, CA 91109, USA.

J. J. Plaut, MS 183-501, Jet Propulsion Laboratory, 4800 Oak Grove, Pasadena, CA 91109, USA.

L. R. Gaddis, U.S. Geological Survey, 2255 N. Gemini Drive, Flagstaff, AZ 86001, USA.

(Received November 20, 2000; revised June 13, 2001;
accepted August 30, 2001.)